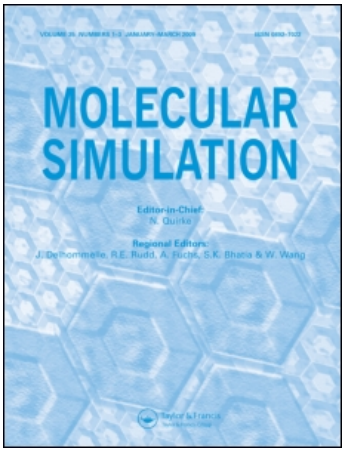

Molecular Simulation
Publication details, including instructions for authors and subscription information:
http://www.informaworld.com/smpp/title~content=t713644482

Influence of odd and even number of Stone-Wales defects on the fracture behaviour of an armchair single-walled carbon nanotube under axial and torsional strain

K. Talukdar[a]; A. K. Mitra[a]
[a] Department of Physics, National Institute of Technology, Durgapur, India

Online publication date: 11 May 2010

To cite this Article Talukdar, K. and Mitra, A. K.(2010) 'Influence of odd and even number of Stone-Wales defects on the fracture behaviour of an armchair single-walled carbon nanotube under axial and torsional strain', Molecular Simulation, 36: 6, 409 — 417
To link to this Article: DOI: 10.1080/08927020903530971
URL: http://dx.doi.org/10.1080/08927020903530971

Molecular Simulation
Vol. 36, No. 6, May 2010, 409–417

Taylor & Francis
Taylor & Francis Group

Influence of odd and even number of Stone–Wales defects on the fracture behaviour of an armchair single-walled carbon nanotube under axial and torsional strain

K. Talukdar and A.K. Mitra*

Department of Physics, National Institute of Technology, Durgapur 713209, India

(*Received 14 September 2009; final version received 4 December 2009*)

Using Brenner's bond-order potential to represent the interaction of the in-plane C—C bond, an armchair (8,8) single-walled carbon nanotube is investigated by molecular dynamics simulation under axial loading and twist, both for perfect and imperfect lattices introducing an increasing number of Stone–Wales (SW) defects. The Young modulus, shear modulus, tensile strength, shear strength, ductility, stiffness and toughness are computed. All the mechanical characteristics are found to change appreciably by the inclusion of SW defects. Two distinct patterns of fracture mode are observed with odd and even numbers of defects. A clear evidence of the defect–defect interaction is observed when more than one defect is included.

Keywords: molecular dynamics simulation; single-walled carbon nanotube; mechanical properties; Stone–Wales defect

PACS: 61.46.Fg; 62.25.−g; 62.25.Mn; 81.07.De

1. Introduction

Extremely fascinating mechanical properties of carbon nanotube (CNT) have attracted the attention of many researchers since the discovery of these high-strength, highly stiff and ductile substances by Iijima [1]. Subsequently, many theoretical studies [2–7] were carried out to explore their mechanical behaviour. A range of Young's modulus values for CNTs from 0.2 to 5.5 TPa, and tensile strength values from 5 to 150 GPa, were calculated by different authors. The mechanical characteristics varied extensively depending on the method of calculation, the chiralities of the nanotubes considered and the interatomic potential functions employed to represent the C—C bond in the plane of the graphene sheet. However, almost all the calculations confirmed that CNTs possessed extraordinarily high tensile strength of the order of TPa, which was at least an order of magnitude higher than the measured values of their tensile strength. Experimental work [8–11] was, however, inadequate owing to the difficulty in setting up an appropriate experimental arrangement to make measurements in the nanoscale. Falvo et al. [10] showed experimentally how a CNT bundle bent or buckled under large strains. The experiments established that the measured lower values of Young's modulus and tensile strength of CNTs were mainly due to the presence of imperfections in them, in particular the Stone–Wales (SW) defects [12]. The presence of topological defects such as the SW defects was verified in the work of Ebbesen and Takada [13] and Miyamoto et al. [14]. The role of vacancy defects in the mechanical properties of CNTs was studied in many theoretical investigations [15–18] and the investigators observed a considerable reduction in strength due to the presence of vacancy defects. Belytschko et al. [19] studied the effect of missing atoms and SW defects using molecular mechanics (MM) and molecular dynamics (MD) simulations.

Decreasing effects on failure stress and failure strain along with the scattering of stress values were reported by Troya et al. [20] for the introduction of one, two and five SW defects that were situated diagonally. A 30–50% reduction in stiffness was found by Chandra et al. [21]. To explore the nucleation of SW defects in single-walled carbon nanotubes (SWCNTs), Lu and Bhattacharya [22] observed the effects of two, four and six defects which were found to change the mechanical properties such as stiffness, strength, etc. of a (6,6) CNT considerably. The effects of odd number of defects were not mentioned in their study. Nardelli et al. [23] found the presence of SW transformation at small strains causing a necking phenomenon and changing the fracture pattern. A hybrid atomistic continuum model was developed by Song et al. [24] to show that the bond breakage precedes the initiation of SW transformation at a strain value of 13%, i.e. much below the inflection occurring at about 30% strain with Brenner's potential. The progressive fracture model of Tserpes and Papanikos [25] used the pairwise modified Morse potential to come to the conclusion that SW defects served as the nucleation site for fracture. They also observed variable reduction in failure stress and failure strain for different types of nanotube, where armchair

*Corresponding author. Email: akmrecdgp@yahoo.com

ISSN 0892-7022 print/ISSN 1029-0435 online

DOI: 10.1080/08927020903530971
http://www.informaworld.com

nanotubes exhibited the largest reduction in failure stress of 18–25% with a reduction in failure strain of 30–41%. The Tersoff–Brenner potential was used by Pozrikidis [26], where the effects of circumferential as well as inclined SW defects were examined extensively for three types of CNT. In the study by Tunvir et al. [27], the interaction of two neighbouring SW defects was investigated. This interaction was found to reduce the failure strength and failure strain by 34 and 70%, respectively. More recently, fracture and progressive failure of graphene sheets and CNTs were predicted by Xiao et al. [28] by the atomistic finite bond element model.

Knowledge of the dependence of various mechanical characteristics of SWCNT on the increasing number of SW defects is useful for the exploitation of CNTs in engineering applications such as high-strength fibre composites. We have carried out MD simulation studies to investigate the dependence of the mechanical characteristics of an armchair (8,8) SWCNT on an increasing number of SW defects both for axial and torsional deformation. It is noteworthy that the modified Morse potential fails to describe the bond breakage as it does not include multibody interactions, although many authors have adopted this potential to describe the fracture mechanism. We have taken the Tersoff–Brenner potential and observed a definite dependence of elastic modulus, tensile/shear strength, failure strain, etc. on the number (one to six) of SW defects. Also, two distinct fracture patterns were observed with odd and even number of defects introduced in the nanotube. The presence of odd number of SW defects has a more pronounced effect on the mechanical characteristics than the presence of even number of defects. This could be explained with the help of the correlation effect between pairs of SW defects.

2. Potential function used

We have used the interatomic potential function developed by Brenner [29] for hydrocarbons, known as the Tersoff–Brenner potential which is of the form

$$E = \sum E_i = \frac{1}{2}\sum_i \sum_{i \neq j} V(r_{ij}),$$

where

$$V(r_{ij}) = f_c(r_{ij})[V^R(r_{ij}) + b_{ij}V^A(r_{ij})].$$

Here, E is the total energy which is decomposed into a site energy E_i which is a function of the bond energy $V(r_{ij})$, where $f_c(r_{ij})$ is a cut-off function that reduces to zero interaction beyond 2.0 Å. $V^R(r_{ij})$ is a pairwise term that models the core–core and electron–electron repulsive interactions and $V^A(r_{ij})$ is a pairwise term that models core–electron attractive interactions, where r_{ij} is the distance between the nearest neighbour atoms i and j, and b_{ij} is a many-body, bond-order term that depends on the number and type of neighbours and bond angles. Although this potential lacks the inclusion of a long-range intermolecular interaction, it enables us to simulate a wide range of deformations of a SWCNT under external loads.

3. Method of calculation

Using the Tersoff–Brenner potential, MD simulation of an (8,8) SWCNT was carried out for increasing axial strain values both for a perfect lattice and with the inclusion of a gradually increasing number of SW defects at some specified locations. The temperature was fixed at 300 K by the Berendsen thermostat. By stretching the tube in small strain increments, the equilibrium potential energy was calculated by the simulation. The force in the lateral dimension was made equal to zero such that the tube was not constrained laterally. We took an (8,8) SWCNT of length 49.19 Å and radius 5.242 Å containing 20 unit cells with 640 atoms. Keeping one end fixed, the other end of the tube was stretched gradually from the unstretched condition. No angular rotation was applied to study the exact influence of the axial strain.

Stress was calculated from the energy–strain curve as $\sigma = 1/V(\mathrm{d}E/\mathrm{d}\varepsilon)$, where σ is the longitudinal stress; V, the volume of the tube; ε, the strain and E, the strain energy of the tube. The volume of the tube is found as $V = 2\pi r \delta r l$, where r is the inner radius of the tube; δr, its wall thickness and l, the length of the tube. We have taken δr as 0.34 nm, which has been the standard value used by most of the authors. To calculate stress from the energy–strain curve, we have used a linear relationship for the elastic region and appropriate nonlinear equations for the segments of high-strain deformation regions. Young's modulus was found from the slope of the linear portion of the stress–strain curve. Toughness of the sample was calculated by finding the area under the stress–strain curve. Length-dependent stiffness was calculated following Xiao and Liao [30], defined as $C = 1/S(\mathrm{d}^2E/\mathrm{d}\varepsilon^2)$, where S is the surface area of the nanotube. The effect of torsion is also studied in our work, considering the same defects in the same tube. The tube is subjected to shear strain ε which is related to the torsion angle θ as $\varepsilon = (r\theta)/l$. Shear stress or torque is calculated using the formula $F = 1/(2\pi h)l^2/r^3\,\mathrm{d}E/\mathrm{d}\theta$. Shear modulus is found from the torque–strain response.

4. Results and discussion

A perfect (8,8) SWCNT in our calculation shows an energy–strain curve as in Figure 1. We have taken into consideration the small changes in the energy–strain curve due to a slight change in the temperature or time step for writing the coordinate file. MD simulation has been performed with five values of temperature (280, 290, 300,

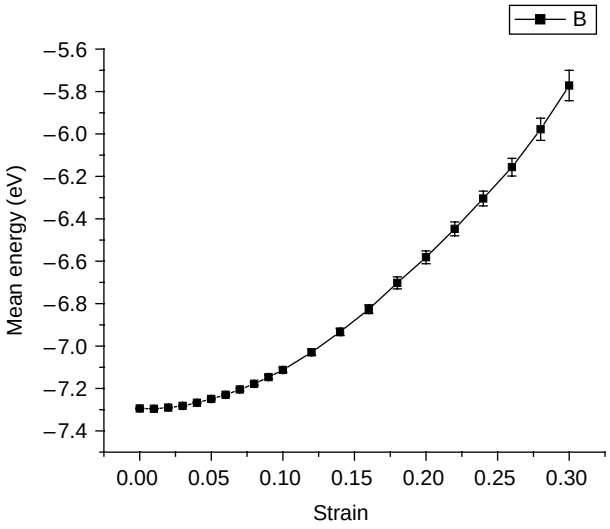

Figure 1. Energy–strain curve for a perfect (8,8) SWCNT. Error bars are indicated by the vertical lines on the graph.

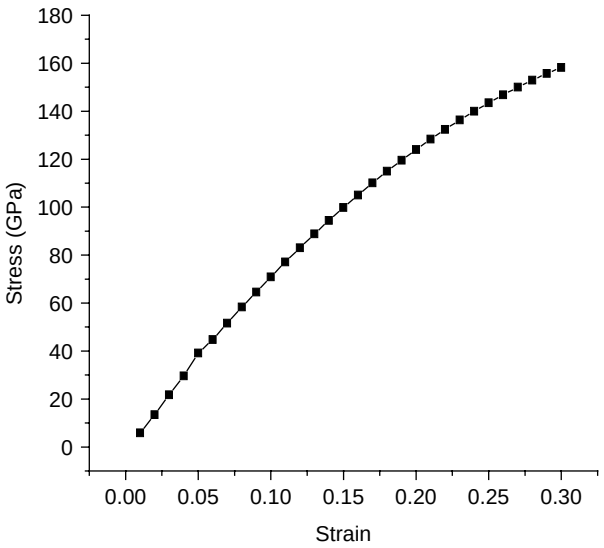

Figure 3. Stress–strain curve for a perfect (8,8) SWCNT.

310 and 320 K) and five values of time step (0.1, 0.3, 0.5, 0.7 and 1.0 ps). The mean of all energies is found to correspond to each strain and error bars are plotted on the mean curve by finding the standard deviation. The result is susceptible neither to small changes in temperature nor to the changes in time steps especially at small strains. For large strains, a slight fluctuation in the energy values is observed but the results are within the error bars as plotted in Figure 1. Our result is compared with the result of Treister and Pozrikidis [31], who also used Brenner's interatomic potential in the energy minimisation process. As evident from Figure 2, our result shows a very good agreement with their data, and thus our MD simulation calculation is validated. A rapid fall in energy is observed at about 30% axial strain where the fracture occurs. Figure 3

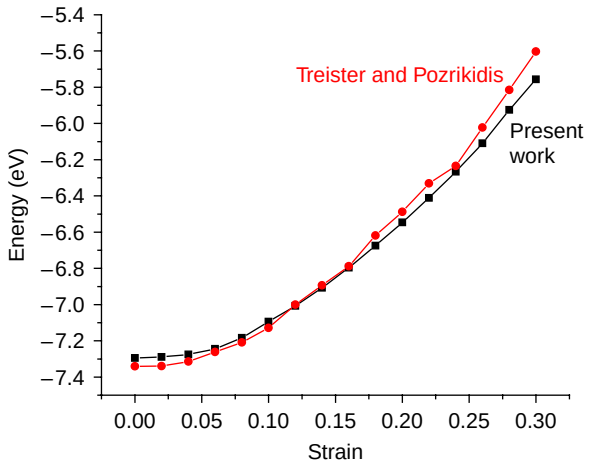

Figure 2. Comparison of our energy–strain curve with that of Treister and Pozrikidis.

shows the stress–strain curve of an ideal (defect-free) (8,8) SWCNT under axial loading. The linear elastic region extends up to 6% strain, beyond which the nature of the curve changes to nonlinearity. The tube shows remarkable ductility and fracture begins at a strain value of 30%. It shows the breaking stress to be 158 GPa and the fracture is brittle. The *Y*-value is calculated from the linear portion of the stress–strain curve and is 0.827 TPa. When the strain reaches 30%, the stress decreases rapidly indicating the onset of rupture in the tube. This result shows a large variation from the experimental work of Yu et al. [32] who observed 10–13% maximum strain and failure stress between 13 and 52 GPa though the experiments were performed with multi-walled carbon nanotubes (MWCNTs), where the individual MWCNT was mounted in between two opposing AFM tips fixed on two cantilever beams and tensile loading is done by moving the upper beam. However, the calculated failure stress is close to the experimental values of Demczyk [33], which is 150 ± 45 GPa for MWCNTs. The DFT calculation of Ogata and Shibutani [34] obtained failure stress for an (8,8) SWCNT as 115 GPa and failure strain as 29.5% with its Young's modulus of 1.01 TPa. For a (5,5) SWCNT, Mielke et al. [15] obtained tensile strength as 135 GPa and strain as 30% in the PM3 [35] approach, 105 GPa and 30% failure strength and failure strain, respectively, with the modified Tersoff–Brenner potential and 110 GPa and 30% with DFT. In all calculations, the maximum strain matches exactly with our calculated value. Jeng et al. [36] obtained these values as 152 GPa and 26% for a (6,6) armchair SWCNT in the tight-binding calculation. Their tensile strength is in very good agreement with our value of 158 GPa. In the MSINDO method [37], Troya et al. [20] obtained a result of 27.9% failure strain and 163 GPa

strength, while, by the PM3 method, 130 GPa of failure stress was reported by them. The *Y*-value as obtained by us is somewhat lower than that of the experimental values of Treacy et al. [8], Wong et al. [9] and Treister and Pozrikidis [31] but matches well with the calculated values of Lu and Bhattacharya [22] (0.851 TPa) for the modified Morse potential, and Troya et al. [20] for the Tersoff–Brenner (0.82 TPa) and modified Tersoff–Brenner (0.82 TPa) potentials. We have studied how an increasing number of the SW defect changes the overall mechanical response of a SWNT. We have taken the Tersoff–Brenner potential for the reason stated earlier. Fracture modes of the CNT with and without defects are also studied elaborately to obtain conclusive results. Such extensive studies were not carried out by earlier authors with this potential. The resistance (stiffness) of 302 J/m^2 is applied by the bulk tube against the applied force. An energy (toughness) of 2.45 J/m^3 is absorbed by the tube during the whole straining process before failure.

With a single defect at the (z, r, θ) value of (-0.61, 5 and 34°), i.e. axially near the origin, the maximum strain dropped to 22% (Figure 4), compared to the failure strain of 30% for a perfect lattice. This lower failure strain may occur due to the following mechanism of plastic deformation and fracture. Straining the defective tube beyond 22% may cause some atoms to be displaced from their equilibrium positions in such a manner that the next nearest neighbours move apart and the interatomic coordination is very much reduced. The line joining the pentagons for a single defect makes an acute angle with the tube axis and thus with the straining direction. Generally, the bond between the pentagons is stronger than the bonds within the pentagons. While stretching the tube axially, elongation of bonds occurs and ultimately the bonds between the pentagons break before failure. The bonds between the heptagons are also very weak and, in the present configuration (Figure 5), these bonds can also break quickly. A reduction of 28 and 26.6% in failure stress and maximum strain, respectively, is observed by the introduction of a single SW defect. The value of Young's modulus is calculated to be 0.785 TPa. With a SW defect, Mielke et al. [15] obtained the failure stress value of 125 GPa compared to our value of 111.25 GPa and 22% maximum strain, the same as obtained by us. The semi-empirical PM3 approach was employed in their study. The modified Morse potential was incorporated by Jiao et al. in their finite element model and by Lu and Bhattacharya in atomistic simulation to obtain Young's modulus, failure strain and failure stress as 0.793 TPa, 89.71 GPa and 8.69% for a (6,6) armchair SWNT, respectively. Tserpes and Papanikos used the same potential in the progressive fracture model and obtained, for (12,12), (5,5) and (18,18) SWCNTs, a tensile strength of nearly about 100 GPa and a maximum strain of about 12%. Failure stress and strain values are lower than those obtained in our calculations mostly due to the choice of the potential. Young's modulus obtained by us is almost the same as that obtained by Lu and Bhattacharya [22] as, in the small strains, the modified Morse potential resembles the Tersoff–Brenner potential. Troya with a single SW defect obtained 24.4% strain in MSINDO and 22.1% in PM3, which is in agreement with our study.

On the contrary, maximum strain is again increased to 26% with two defects introduced in the positions (9.84, 5.38, 22) and (-9.84, 5.38, 22). Although Young's modulus is reduced to 0.779 TPa, a very marginal change in tensile strength from the value of a perfect tube is observed with two defects (Figure 6). However, reduction in stiffness and toughness proves an overall degradation in mechanical response. According to Lu and Bhattacharya, two defects result in a *Y*-value equal to 0.771 TPa, whereas we have obtained 0.779 TPa, 83.11 GPa and 7.2% failure stress and failure strain which in their study are much

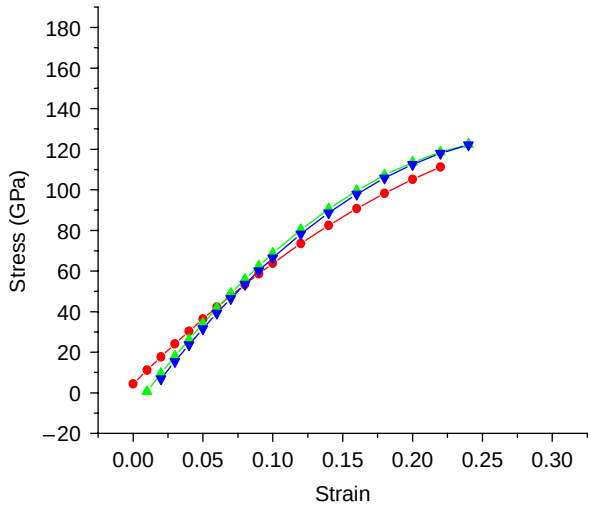

Figure 4. Stress–strain curves for an (8,8) SWCNT with one (red), three (green) and five (blue) defects (colour online).

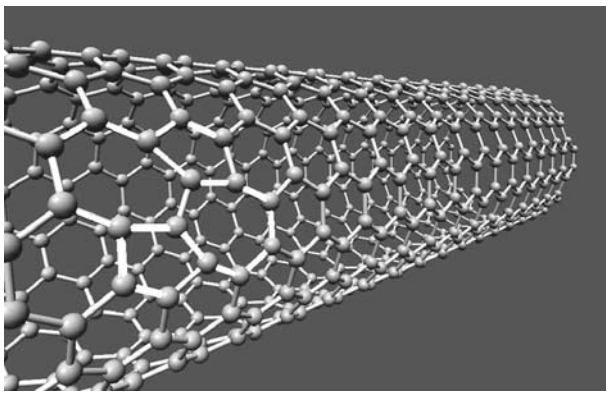

Figure 5. An (8,8) SWCNT with one SW defect.

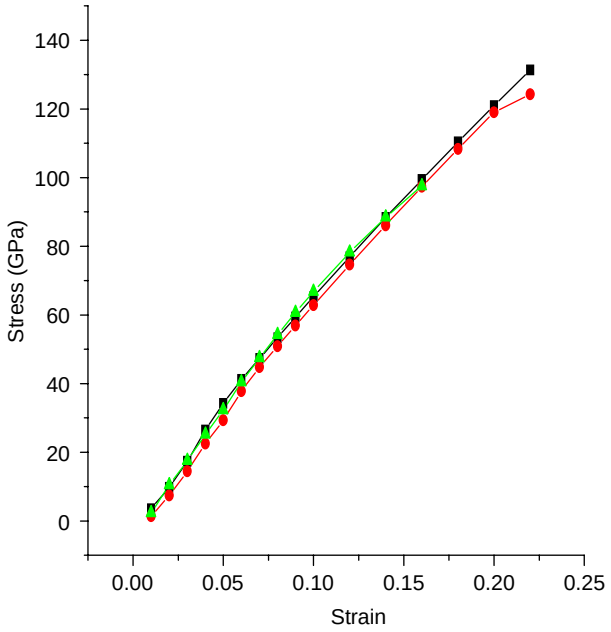

Figure 6. Stress–strain curves for an (8,8) SWCNT with two (black line), four (red line) and six (green line) defects (colour online).

lower than that obtained by us (Table 1). The reason for this is the non-resemblance of the modified Morse potential to the Tersoff–Brenner potential at high strain where the former potential does not give a reasonable result. Troya obtained 24.1% maximum strain with two SW defects with MSINDO. In spite of some same kind of works, none of the authors to our knowledge before us have obtained such difference in the results for one and two defects. The gradual degradation of the mechanical properties was observed by Troya et al. [20] and Lu and Bhattacharya [22]. The increase in maximum strain and stress for two defects when compared with the values for one defect clearly shows the defect–defect interaction during the deformation process. According to Samsonidze et al. [38], the defect–defect interaction energy may be attractive or repulsive depending on the angular orientation between the parallel defects. Actually, 5/7/7/5 is a source of edge dislocation which can result in a dislocation glide. Diagonally situated parallel defects, which are situated next to each other, are energetically most favourable. Both attraction and repulsion are possible between two such defects. If attraction occurs, the moving dislocations pile up such that the energy of the system slowly decreases due to the application of the external force. On the other hand, any external force should bring the system to the minimum energy state easily if the repulsive interaction acts between the defects. However, we have defined two well-separated defects randomly on the same line (Figure 7), where the line joining the two pentagons is parallel to the tube axis. This configuration helps an armchair SWCNT to release its excess strain of formation of defects in the loading direction. Formation energy of the SW defect is very high, a few electron volts. By the application of axial strain, the energy of the system comes down by breaking the bonds within the pentagons which are parallel to the straining direction as that needs less energy. However, the process is comparatively slower than that of the single defect case. Here, though the bonds within the pentagons break first, the dislocation cores of the two defects cannot split them sufficiently for the repulsive interaction between them which is possible for the cylindrical geometry of the tube, i.e. the curvature. Since the defects here are on the same line, the curvature does not play a significant role in their interaction. So, the dislocation dipoles prefer to merge together to result in an attractive correlation. As a result, the system shows larger failure strain or failure stress.

Thus, it can be concluded that, for one defect, the reduction of mechanical properties is more pronounced as there is no interference by other defects and the breaking process shows that the defect site acts as a source of initiation of the fracture of the tube. In the case of the attraction between two interacting defects, the breaking of the tube starts near one end where one of the defects is located. The defect–defect correlation thus leads to such results and also causes the increase in maximum strain or failure stress in comparison with the one defect situation.

The existence of the correlation between the defects is further established in another way when we put three defects in the nanotube in positions (0, 5.38, 22), (15.99, 5.38, 45) and (−15.99, 5.38, 45). Young's modulus is increased to 0.821 TPa, and ductility and tensile strength

Table 1. Young's modulus, tensile strength, maximum strain, stiffness and toughness at failure of an (8,8) SWCNT with increasing number of defects.

	Without defect	One defect	Two defects	Three defects	Four defects	Five defects	Six defects
Young's modulus (TPa)	0.827	0.785	0.779	0.821	0.739	0.744	0.747
Failure stress (tensile strength; GPa)	158.26	111.25	151.2	122.39	149.57	122.14	122.1
Maximum strain (ductility)	30%	22%	26%	24%	26%	24%	24%
Stiffness (J/m^2)	302	264.89	274	274.1	247.82	248.68	258.92
Toughness (J/m^3)	2.76	1.43	2.07	1.74	2.01	1.69	1.7

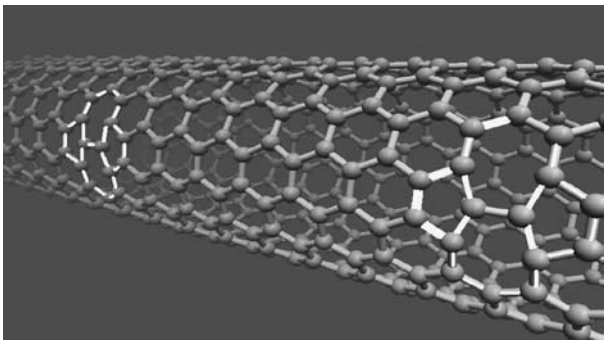

Figure 7. Two SW defects shown in an (8,8) SWCNT.

are also reduced by 20 and 22.7%, respectively (Figure 4). Three defects have reduced the toughness to 1.74 J/m^3 but could not change the stiffness from its previous value. The breaking process for three defects (Figure 8(a)) is similar to the case with one defect.

The effect of four defects in the z, r, θ positions (−9.84, 5.38, 22), (−20.91, 5.38, 45), (9.84, 5.38, 22) and (20.91, 5.38, 45) resembles almost that of two defects. The results of the inclusion of five (Figure 4) and six (Figure 6) defects are more or less similar to the result of three and four defects, respectively, with more complex interaction between several defects. The results are tabulated in Table 1. The relation of the strain energy (E) and the number of defect (n) for small strain (up to 4%) is

$$E = a + bn + cn^2,$$

where a, b and c are constant terms.

For the higher strain values, the relation is more complicated and includes fifth- or sixth-order terms. For four defects, Young's modulus, failure stress and failure strain of 0.738 TPa, 76.29 GPa and 5.5%, respectively, are noticed by Lu and Bhattacharya and, for six defects, these values are 0.716 TPa, 74.56 GPa and 4.94%. In Troya's calculation, failure strains are 26.6% with MSINDO and 21.4% with PM3 with five SW defects. It can be said that when the tube is stretched, the energies of the pristine and defective tubes are increased at small strains (Figure 9). On increasing the strain, many bonds are broken gradually, atoms are displaced with necking of the tube and ultimately the tube breaks. The odd and even number of defects shows two different patterns of fracture modes. The fractures in all cases are brittle in nature. For the odd number of defects, as in Figure 8(a), the necking is sharp and fracture occurs at smaller strains than that with the even number of defects as shown in Figure 8(b). This proves the positive correlation between more than one collinear defect. The dislocation cores of the defects merge together resulting in such phenomena.

Clearly, we find two different types of breaking mechanisms. With the odd number of defects, the tube breaks in the middle where one defect is situated. But with the even number of defects, the fracture originates near the end at one defect site. Certainly, the defect–defect positive interaction, i.e. attraction, has occurred for the even number of defects leading to such a result. For the odd number of defects, it seems that the defect situated in the

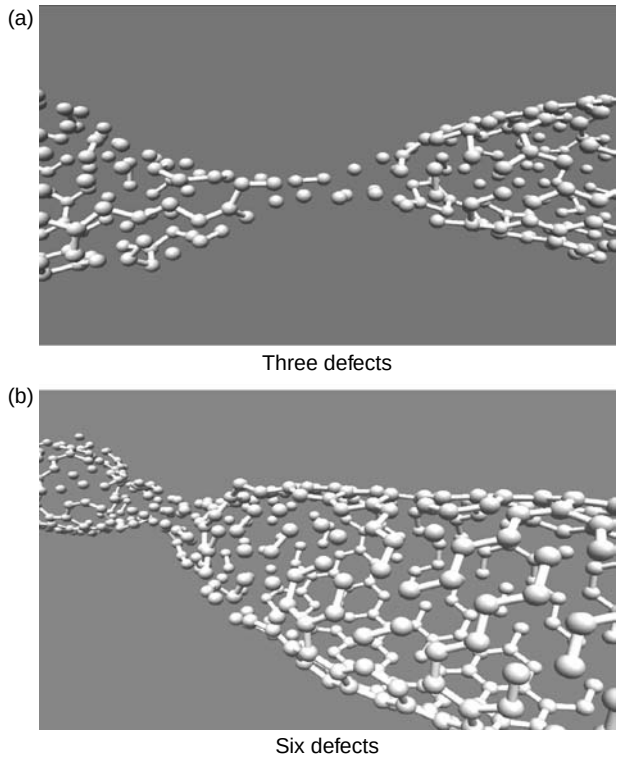

Figure 8. Modelling of fracture mechanisms of an (8,8) SWCNT with odd and even number of defects.

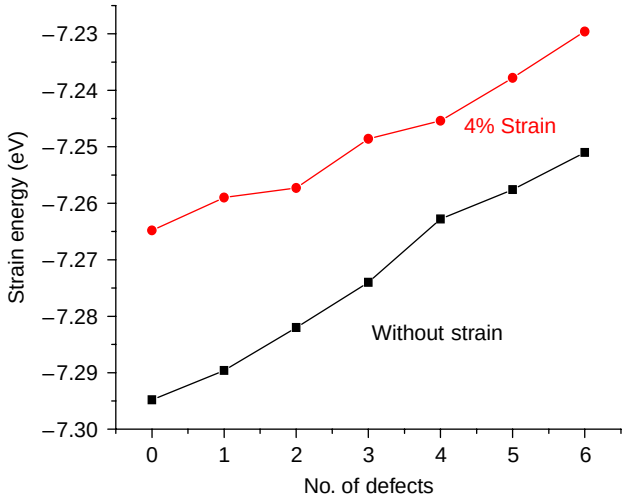

Figure 9. Variation of strain energy with increasing number of defects.

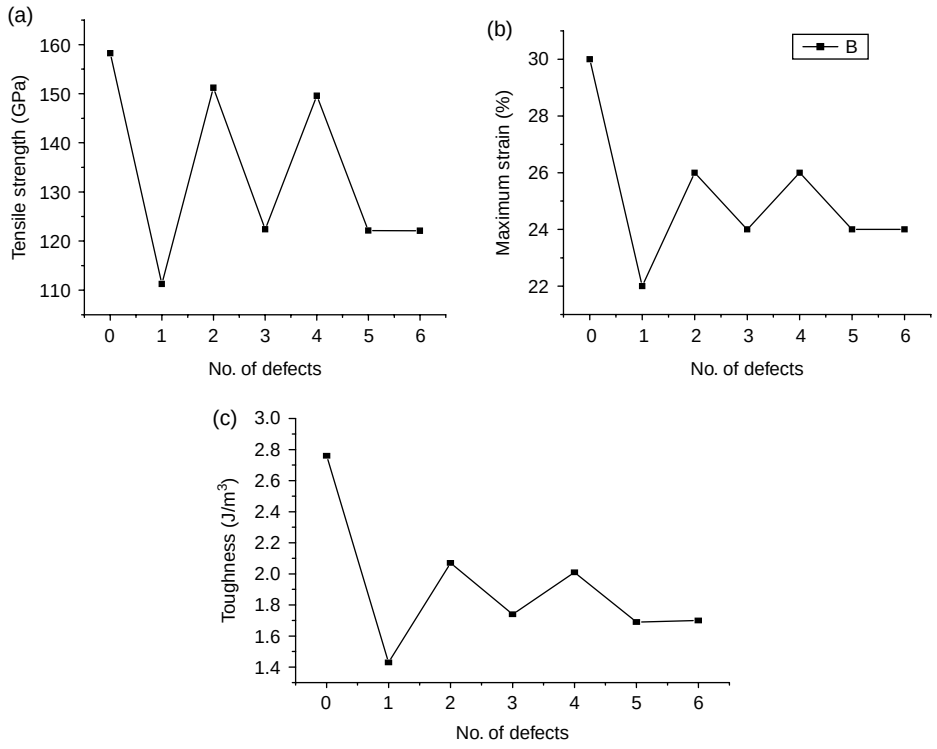

Figure 10. Variation of tensile strength, maximum strain and toughness of an (8,8) SWCNT with the number of defects.

Table 2. Shear modulus, maximum shear stress and maximum shear strain of an (8,8) SWCNT with increasing number of defects.

	Without defect	One defect	Two defects	Three defects	Four defects	Five defects	Six defects
Shear modulus (TPa)	0.532	0.51	0.53	0.524	0.487	0.522	0.495
Maximum shear stress (GPa)	33.6	28.5	32.23	30.13	28.5	30.2	28.8
Maximum shear strain	6%	5%	5%	6%	5%	5%	5%

middle was acted upon by other defects situated at both sides and thus its fracture behaviour was different.

Figure 10 shows that the nature of variation of tensile strength, maximum strain and toughness with the number of defects is more or less similar, showing higher values for the even number of defects. Fluctuation of the values decreases for a larger number of defects.

The effect of torsion is also studied in our work. Shear strain is applied on the tube without defects and also with defects introduced into them. Gradually, the tube is twisted and energy is minimised in each step of twist applied. The shear modulus of a perfect (8,8) CNT is calculated as 0.532 TPa (Table 2). A single defect reduces the strength and maximum shear stress considerably. An increase in these values is observed in the case of two defects. The stress–strain responses with odd and even number of defects are shown in Figures 11 and 12. From these figures, it is clear that the results of one and five defects are similar and also the results of two and four defects resemble

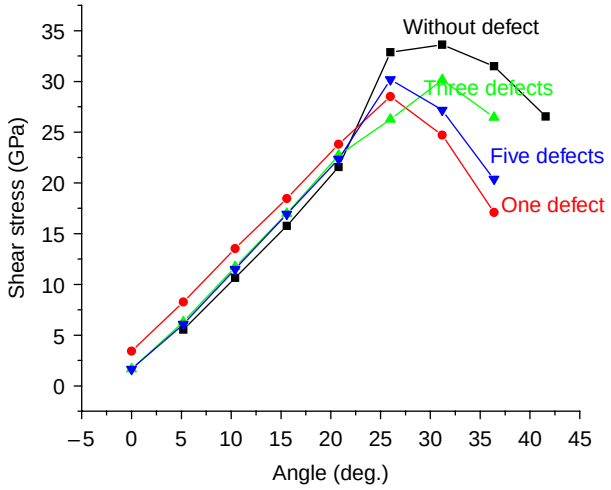

Figure 11. Shear stress–strain response of an (8,8) SWCNT with one, three and five defects.

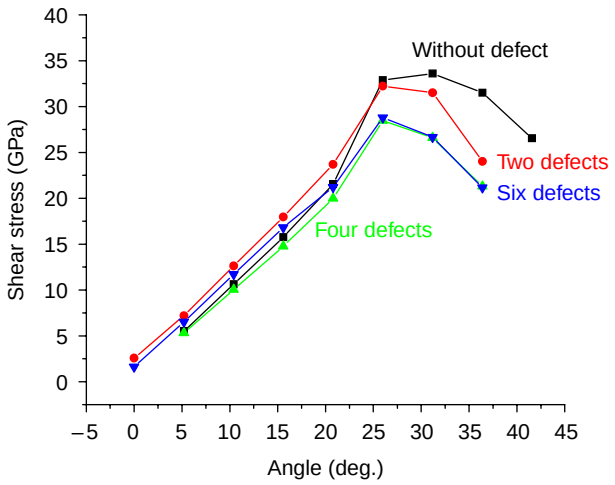

Figure 12. Shear stress–strain response of an (8,8) SWCNT with two, four and six defects.

each other. The value of the shear modulus is closer to 0.45 TPa, calculated by Lu [39] using an empirical force constant model. The result is also in proximity of the results of Wang et al. [40] by the MD simulation and Xiao et al. [41] by the MM calculation. The deformation of the tube on application of twist is shown in Figure 13(a). Twist can be applied up to an angle of 31° for a perfect tube and, for defective tubes, the angle is 26°. Figure 13(b) shows that twisting the tube by a large angle deforms into a shape that prevents further twisting.

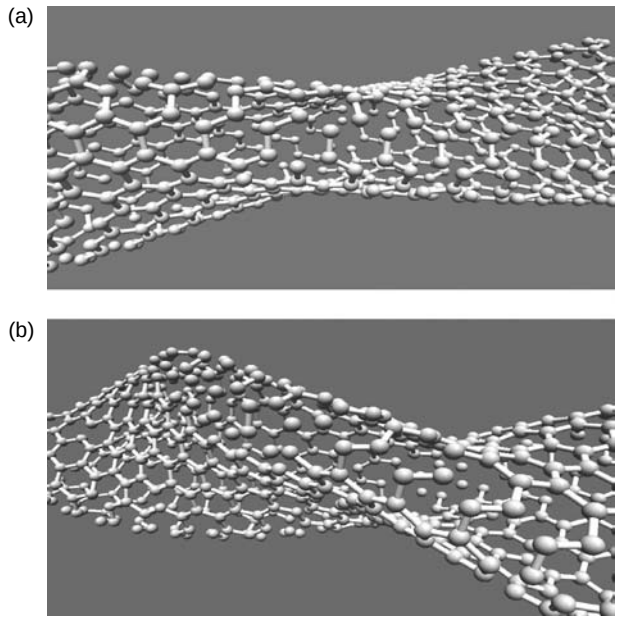

Figure 13. Deformation of an (8,8) SWCNT with shear strain for (a) a small angle and (b) a comparatively large angle.

In the case of two or more number of defects being present in the tube, the influence of defects on the mechanical properties of the tube is less pronounced than in the presence of a single defect, due to the interaction and correlation between the defects. Although a slight increase in the maximum shear stress in the case of five defects is observed, most of the results of torsion show the difference in results between the odd and even number of defects for at least up to three defects. However, the breaking of the tube is not so sharp with torsion and no remarkable change in the maximum failure strain is observed with increasing number of defects. Here, shear strain changes the nature of the correlation between the defects in a complicated manner for a larger number of defects.

5. Conclusions

By the above study on the role of SW defects in the mechanical properties of an armchair (8,8) SWCNT, we may conclude that the SW defects change the overall pattern of mechanical behaviour of SWCNTs in a significant manner. The failure stresses and failure strains are substantially changed both in the case of axial stretch and twist. For axial strain, the effect of one defect is maximum giving a failure strain value of 22%, i.e. the failure strain value is reduced by 26.6% from the value of a perfect tube. The tensile strength is reduced by a maximum of 47.01 GPa as compared with that of the perfect tube, i.e. the reduction is 30%. The *Y*-value is changed only by an amount of 5% for one defect, 5.8% for two defects, 7% for three defects, 10.6% for four defects and 10 and 9.6% for five and six defects, respectively. For twist, the maximum stress reduces by 15.17% for one defect and 4 and 8.5% for two and three defects, respectively. Thus, the influence of the correlation between the defects in SWCNTs is established for both axial and angular strain.

References

[1] S. Iijima, *Helical microtubules of graphitic carbon*, Nature 354 (1991), pp. 56–58.
[2] B.I. Yakobson, C.J. Brabec, and J. Bernholc, *Nanomechanics of carbon tubes: Instabilities beyond linear response*, Phys. Rev. Lett. 76 (1996), pp. 2511–2514.
[3] B.I. Yakobson, *Mechanical relaxation and intramolecular plasticity in carbon nanotubes*, Appl. Phys. Lett. 72 (1998), pp. 918–920.
[4] K.M. Liew, C.H. Wong, X.Q. He, M.J. Tan, and S.A. Meguid, *Nanomechanics of single and multiwalled carbon nanotubes*, Phys. Rev. B 69 (2004), p. 115429.
[5] R.C. Batra and A. Sears, *Uniform radial expansion/contraction of carbon nanotubes and their tranverse elastic moduli modelling*, Simul. Mater. Sci. Eng. 15 (2007), pp. 835–844.
[6] V.R. Coluci, N.M. Pugno, S.O. Dantas, D.S. Galvao, and A. Jorio, *Atomistic simulations of the mechanical properties of 'super' carbon nanotubes*, Nanotechnology 18 (2007), 335702.
[7] G. Dereli and C. Ozdogan, *Structural stability and energetics of single-walled carbon nanotubes under uniaxial strain*, Phys. Rev. B 67 (2003), 035416.

[8] M.M.J. Treacy, T.W. Ebbesen, and J.M. Gibson, *Exceptional high Young's modulus observed for individual nanotubes*, Nature 381 (1996), pp. 678–680.
[9] E.W. Wong, P.E. Sheehan, and C.M. Lieber, *Nanobeam mechanics: Elasticity, strength and toughness of nanorods and nanotubes*, Science 277 (1997), pp. 1971–1975.
[10] M.R. Falvo, G.J. Clary, R.M. Taylor, V. Chi, F.P. Brooks, S. Washburn, and R. Superfine, *Bending and buckling of carbon nanotubes under large strain*, Nature 389 (1997), pp. 582–584.
[11] A. Krishnan, E. Dujardin, T.W. Ebbesen, P.N. Yianilos, and M.M.J. Treacy, *Young's modulus of single-walled nanotubes*, Phys. Rev. B 58 (1998), pp. 14013–14019.
[12] A.J. Stone and D.J. Wales, *Theoretical studies of icosahedral C_{60} and some related species*, Chem. Phys. Lett. 128 (1986), pp. 501–503.
[13] T.W. Ebbesen and T. Takada, *Topological and sp^3 defect structures in nanotubes*, Carbon 33 (1995), pp. 973–978.
[14] Y. Miyamoto, A. Rubio, S. Berber, M. Yoon, and D. Tomanek, *Spectroscopic characterizaion of Stone–Wales defects in nanotubes*, Phys. Rev. B 69 (2004), 121413(R).
[15] S.L. Mielke, D. Troya, S. Zhang, J.L. Li, S. Xiao, R. Car, R.S. Ruoff, G.C. Schatz, and T. Belytschko, *The role of vacancy defects and holes in the fracture of carbon nanotubes*, Chem. Phys. Lett. 390 (2004), pp. 413–420.
[16] G.D. Lee, C.Z. Wang, E. Yoon, N.M. Hwang, and K.M. Ho, *Vacancy defects and the formation of local haecklite structures in graphene from tight-binding molecular dynamics*, Phys. Rev. B 74 (2006), 245411.
[17] W. Hou and S. Xiao, *Mechanical behaviors of carbon nanotubes with randomly located vacancy defects*, J. Nanosci. Nanotech. 7 (2007), pp. 4478–4485.
[18] Q. Wang, W.H. Duan, N. Richards, and K.M. Liew, *Modeling of fracture of carbon nanotubes with vacancy defects*, Phys. Rev. B 75 (2007), 201405.
[19] T. Belytschko, S.P. Xiao, G.C. Schatz, and R. Ruoff, *Atomistic simulations of nanotube fracture*, Phys. Rev. B 65 (2002), 235430.
[20] D. Troya, S.L. Mielke, and G.C. Schatz, *Carbon nanotube fracture - differences between quantum mechanical mechanisms and those of empirical potentials*, Chem. Phys. Lett. 382 (2003), pp. 133–141.
[21] N. Chandra, S. Namilae, and C. Shet, *Local elastic properties of carbon nanotubes in the presence of Stone–Wales defects*, Phys. Rev. B 69 (2004), 094101.
[22] Q. Lu and B. Bhattacharya, *Effect of randomly occurring Stone–Wales defects on mechanical properties of carbon nanotubes using atomistic simulation*, Nanotechnology 16 (2005), pp. 555–566.
[23] B.I. Nardelli, B.I. Yakobson, and J. Bernholc, *Mechanism of strain release in carbon nanotubes*, Phys. Rev. B 57 (1998), pp. R4277–R4280.
[24] J. Song, H. Jinag, and D.L. Shi, *Stone–Wales transformation: Precursor of fracture in carbon nanotubes*, Int. J. Mech. Sci. 48 (2006), pp. 1464–1470.
[25] K.I. Tserpes and P. Papanikos, *The effect of Stone–Wales defect on the tensile behavior and fracture of single-walled carbon nanotubes*, Compos. Struct. 79 (2007), pp. 581–589.
[26] C. Pozrikidis, *Effect of the Stone–Wales defect on the structure and mechanical properties of single-wall carbon nanotubes in axial stretch and twist*, Arch. Appl. Mech. 79 (2009), pp. 113–123.
[27] K. Tunvir, A. Kim, and S.H. Nahm, *The effect of two neighboring defects on the mechanical properties of carbon nanotubes*, Nanotechnology 19 (2008), 065703.
[28] J.R. Xiao, J. Staniszewski, and J.W. Gillespie, Jr, *Fracture and progressive failure of defective graphene sheets and carbon nanotubes*, Compos. Struct. 88 (2009), pp. 602–609.
[29] D.W. Brenner, *Empirical potential for hydrocarbons for use in simulating the chemical vapour deposition of diamond films*, Phys. Rev. B 42 (1990), pp. 9458–9471.
[30] T. Xiao and K. Liao, *Nonlinear elastic properties of carbon nanotubes subjected to large axial deformations*, Phys. Rev. B 66 (2002), 153407.
[31] Y. Treister and C. Pozrikidis, *Numerical study and equilibrium shapes and deformations of single-wall carbon nanotubes*, Comput. Mater. Sci. 41 (2008), pp. 383–408.
[32] M.F. Yu, B.S. Files, S. Arepalli, and R.S. Ruoff, *Tensile loading of ropes of single wall carbon nanotubes and their mechanical properties*, Phys. Rev. Lett. 84 (2000), pp. 5552–5555.
[33] B.G. Demczyk, *Direct mechanical measurement of the tensile strength and elastic modulus of multiwalled carbon nanotubes*, Mater. Sci. Eng. A 334 (2002), pp. 173–178.
[34] S. Ogata and Y. Shibutani, *Ideal tensile strength and band gap of single-walled carbon nanotubes*, Phys. Rev. B 68 (2003), 165409.
[35] J.J.P. Stewart, *Optimization of parameters for semiempirical methods I. Method*, J. Comput. Chem. 10 (1989), pp. 209–220.
[36] Y.R. Jeng, T. Ping-Chi, and F. Te-Hua, *Effects of temperature and vacancy defects on tensile deformation of single-walled carbon nanotubes*, J. Phys. Chem. Solids 65 (2004), pp. 1849–1856.
[37] B. Ahlswede and K. Jug, *Consistent modifications in SINDO1. I. Approximations and parameters*, J. Comp. Chem. 20 (1999), pp. 563–571.
[38] Ge.G. Samsonidze, G.G. Samsonidze, and B.I. Yakobson, *Energetics of Stone–Wales defects in deformations of monoatomic hexagonal layers*, Comput. Mater. Sci. 23 (2002), pp. 62–72.
[39] J.P. Lu, *Elastic properties of nanotubes and nanoropes*, Phys. Rev. Lett. 79 (1997), pp. 1297–1300.
[40] L.F. Wang, Q.S. Zheng, J.Z. Liu, and Q. Jiang, *Size dependence of the thin-shell model for carbon nanotubes*, Phys. Rev. Lett. 95 (2005), 105501.
[41] J.R. Xiao, B.A. Gama, and J.W. Gillaspie, *An analytical molecular structural mechanics model for the mechanical properties of carbon nanotubes*, Int. J. Solids Struct. 42 (2005), pp. 3075–3087.